Check for updates

Chemistry–A European Journal
Research Article
doi.org/10.1002/chem.202301867
Chemistry Europe
European Chemical Societies Publishing
www.chemeurj.org

Tunable Regioselectivity in C–H-Activated Direct Arylation Reactions of Dithieno[3,2-*b*:2′,3′-*d*]pyrroles

Astrid Vogt,[a] Florian Stümpges,[a] Jessi Bajrami,[a] Daniel Baumgarten,[a] Judith Millan,[b] Elena Mena-Osteritz,[a] and Peter Bäuerle*[a]

Dedicated to Prof. Andrew B. Holmes (University of Melbourne, Australia) on the occasion of his 80th birthday

In this study, regioselectively controlled direct arylation of dithieno[3,2-*b*:2,3′-*d*]pyrroles (DTPs) is reported. By carefully selecting the catalytic system, Pd source, ligand, and additives, we achieved either selective N-arylation or unprecedented β-arylation and β,β′-diarylation of the DTP core through C–H activation when reacting unsubstituted *H*-DTP with 9-anthracenyl halides. For N-substituted DTPs, we obtained regioselective carboxylate-assisted arylation of the α-position(s). Consequently, depending on the catalytic system and substitution at the DTP nitrogen, we successfully synthesized novel regioselectively substituted DTPs, including N-aryl, rarely reported β-aryl, β,β′-diaryl, α-aryl, and α,α′-diaryl scaffolds. These compounds can be straightforwardly prepared and further functionalized for applications as organic electronic materials.

Introduction

In the coupling of (hetero)aryls with aryl halides, Pd-catalyzed C–H activation has become wide-spread for the effective preparation of organic materials, in particular for conjugated (donor–acceptor) oligomers or polymers, due to the avoidance of metalated species.[1–4] In this respect, thiophenes and thiophene-based building blocks are represented in many advanced materials for organic electronic applications and typically are connected via the α-positions, which provide full π-conjugation and are more reactive in direct (hetero)arylation reactions.[5,6] If in aryl halide/thiophene C–H couplings both, α- and β-positions at the thiophene are available, unselective C–H activation of the β-position might occur and often lead to defects even in small quantities, for example, in thiophene-based polymers, which should be avoided because they influence the physical properties.[7,8] Even though calculations have shown for various scaffolds such as (substituted) thiophenes, benzo[*b*]thiophenes, or benzodithiophenes that the Gibbs free energy of activation for the insertion of Pd into the α-C–H bond is smaller by 3–4 kcal mol^{-1} compared to the β-C–H bond, the challenge of regioselectivity remains.[4,5,8,9]

On the other hand, the extension of conjugated π-systems of thiophenes by selective β-C–H functionalization represents an interesting alternative for the growing area of organic electronic materials. In this respect, in seminal work Itami and co-workers have developed a general catalytic system for the β-selective arylation of thiophenes with iodoarenes. 2,3-, 3-, and 2-substituted thiophenes, benzo[b]thiophene, and thienothiophene were phenylated in high C4 (β)-selectivity vis-à-vis the C5 (α)-position with the catalytic system $PdCl_2$/$P[OCH(CF_3)_2]_3$ and silver carbonate. Most interestingly, thiophene itself was reacted with the same catalytic system to 3-phenylthiophene in a regioselectivity of 88:12 (β/α). By changing the ligand to tricyclohexylphosphane (PCy_3) or 1,2-bis(diphenylphosphino)ethane (dppe) the β/α-ratio was controlled and completely reversed to $<$1:99 whereby 2-phenylthiophene was obtained in high yield.[10] The mechanism of Itami's ligand-controlled α/β-selective Pd-catalyzed activation/arylation of thiophenes was computationally investigated by Fu et al. Besides classical aromatic substitution (S_EAr), carboxylate-assisted metalation-deprotonation (CMD) or Heck-type mechanisms were taken into account.[11] Other contributions extending the scope of β-selective C–H bond arylation of thiophenes and benzo[*b*]thiophenes were published by Bach,[12] Studer and Itami,[13] Oi,[14] Doucet,[15] Larrosa,[16] Glorius,[17] and Yu.[18]

Larger thiophene-based heteroacene systems have been rather rarely subjected to direct arylation reactions. Among them, thienothiophene,[10b] benzodithiophenes,[19] dithienosilole, dithienocyclopentadiene, dithienobenzotropone,[5] and indacenodithiophene[20] clearly showed preferential substitution at the α-positions. In the case of related *S,N*-heteroacenes[21] direct arylation reactions of N-substituted dithieno[3,2-*b*:2,3′-*d*]pyrrole (DTP) have been only recently described for the first time.

[a] *A. Vogt, F. Stümpges, J. Bajrami, D. Baumgarten, Dr. E. Mena-Osteritz, Prof. Dr. P. Bäuerle*
Institute of Organic Chemistry II and Advanced Materials
University of Ulm
Albert-Einstein-Allee 11, 89081 Ulm (Germany)
E-mail: peter.baeuerle@uni-ulm.de

[b] *Dr. J. Millan*
Dpto. de Química - Facultad de Ciencia y Tecnología
Universidad de La Rioja
Madre de Dios 53, 26006 Logroño-La Rioja (España)

Supporting information for this article is available on the WWW under https://doi.org/10.1002/chem.202301867

© 2023 The Authors. Chemistry - A European Journal published by Wiley-VCH GmbH. This is an open access article under the terms of the Creative Commons Attribution Non-Commercial NoDerivs License, which permits use and distribution in any medium, provided the original work is properly cited, the use is non-commercial and no modifications or adaptations are made.

© 2023 The Authors. Chemistry - A European Journal published by Wiley-VCH GmbH

15213765, 2023, 60, Downloaded from https://chemistry-europe.onlinelibrary.wiley.com/doi/10.1002/chem.202301867 by Universidad de la Rioja, Wiley Online Library on [29/11/2023]. See the Terms and Conditions (https://onlinelibrary.wiley.com/terms-and-conditions) on Wiley Online Library for rules of use; OA articles are governed by the applicable Creative Commons License

Nguyen et al. used N-benzoyl-DTP in direct arylation copolymerizations with triphenylamine or triphenylbenzene for the preparation of hyperbranched polymers. Connection of the DTP units by the α-positions in the polymer was deduced from NMR spectra.[22] Dessi et al. developed donor–acceptor dyes based on N-alkylated and N-arylated DTP units. Pd-catalyzed direct arylation with brominated benzothiadiazoles led in the case of N-hexyl-DTP to inseparable mixtures of α/β-substituted DTPs, whereby the sterically more hindered N-biphenyl-DTP delivered α-selective products.[23]

DTPs represent highly interesting and frequently used multifunctional and electron-rich building block in organic semiconducting materials for application in organic electronic devices[24–31] or in polymeric form as electrode material in rechargeable batteries.[32,33] DTPs are typically synthesized by Pd-catalyzed Buchwald–Hartwig amination/cyclization of 3,3′-dibromo-2,2′-bithiophene precursors and alkyl or aryl amines to form the central pyrrole ring.[34] We recently extended the scope of N-substituted DTPs by Pd- or Cu-catalyzed coupling of *H*-DTP **1** with well available aryl, acene, and heterocyclic halides resulting in a series of N-arylated and N-heteroarylated DTPs, which were subsequently implemented into functional materials for single material organic solar cells[35] or as hole transport material for perovskite solar cells,[36] respectively.

In this contribution, we describe the deeper investigation of the reaction of unsubstituted *H*-DTP **1** with 9-anthracenyl halides **2**. By serendipity we found that by proper choice of the catalytic system instead of the expected N-arylation[35] unprecedented direct β-arylation or β,β′-diarylation of the DTP core by regioselective C–H activation is achieved (Scheme 1). When we apply N-substituted DTPs **6**, instead, regioselective and carboxylate-assisted direct arylation of the α-positions is obtained. Thus, by the proper choice of catalytic system and depending on the substitution at the DTP nitrogen, novel differently substituted DTPs with *N*-(9′-anthryl), β-(9′-anthryl), β,β′-di (9′-anthryl), α-(9′-anthryl), and α,α′-di (9′-anthryl) scaffolds become available. In this respect, we could broaden the general scope and methodology of preparing DTP derivatives, which might be interesting as building block for the preparation of organic semiconducting materials. In particular, β- and β,β′-substituted DTPs are rarely described in literature and only 3,5-dimethyl[37] and 3,5-didodecyl-DTPs have been reported.[38] In the case of α- and α,α′-arylated DTPs, our direct arylation method facilitates their preparation by replacing the typically used metalated or halogenated DTPs in transition metal-catalyzed coupling reactions.[29,39]

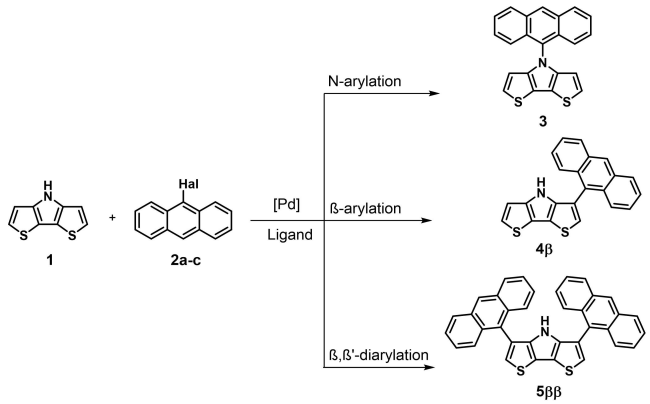

Scheme 1. Spectrum of arylation products by reacting *H*-DTP **1** and 9-anthracenyl halides **2** under Pd catalysis.

Results and Discussion

Direct arylation reactions of *H*-DTP 1: Ligand and Pd source screening

In order to assess the unprecedented β-selectivity for direct arylation reactions of *H*-DTP **1**, we screened and tested various catalytic systems, additives, and reaction conditions to optimize yields and regioselectivities of the arylation products. Typically, the reactions were conducted in closed vials under inert gas by reacting one equivalent (equiv.) of *H*-DTP **1**, 2.1 equiv. of 9-bromoanthracene **2**, and 1.5 equiv. of sodium *tert*-butylate (NaO*t*Bu) in toluene for 6 days at 110 °C. After work-up, the product mixtures were separated by preparative HPLC and yields are given as isolated yields of pure products.

Among the 15 ligands tested, tris(dibenzylideneacetone)dipalladium(0) (Pd_2dba_3) as Pd source, 4,5-bis(diphenylphosphino)-9,9-dimethylxanthene (Xantphos), and 2-dicyclohexylphosphino-2′,6′-dimethoxybiphenyl (SPhos) gave the best results with respect to the formation of N-arylated DTP **3** (63% and 48% yield, respectively). Most of the other tested ligands showed low or no reactivity. Furthermore, the screening revealed that the system Pd_2dba_3/Xantphos gave the best overall yield (86%) and provided β-selective DTP core arylation of **1** to (9′-anthryl)-DTP **4β** in 23% yield. 2,2′-Bis(diphenylphosphino)-1,1′-binaphthyl (BINAP) as ligand gave the highest combined yield of DTP **4β** (43%) and twofold β-substituted DTP **5ββ** (8%) without the formation of N-substituted DTP **3**. Besides BINAP, tri-*tert*-butylphosphine (tBu_3P) was similarly effective as ligand and led to an increased amount of disubstituted product **5ββ** (17%) compared to **4β** (33%; Scheme 1, Table S1 in the Supporting Information)

In the next round of screening, we complemented Pd_2dba_3 as Pd source with palladium(II)-acetate ($Pd(OAc)_2$), tris(dibenzylideneacetone)dipalladium ($Pd(dba)_2$), bis(tri-*tert*-butylphosphine)palladium(0) $Pd(tBu_3P)_2$, or bis(triphenylphosphine)palladium chloride ($Pd(PPh_3)_2Cl_2$) and used the most active ligands from the prior optimization round. With respect to the N-arylation reaction, $Pd(dba)_2$/Xantphos slightly excelled the above discussed Pd_2dba_3/Xantphos catalyst and N-(9′-anthryl)-DTP **3** was formed in 68% yield. $Pd(OAc)_2$/Xantphos provided slightly less DTP **3** (63%), but the highest overall yield (98%) due to the additional formation of β-substituted DTP **4β** (35%). The catalyst $Pd(PtBu_3)_2$ turned out to be the most reactive in the series of β-arylation reaction. Thus, with BINAP as ligand, quite selectively DTP **4β** was isolated in 66% yield. Under these conditions, the twofold β,β′-arylated DTP **5ββ** was best formed with the catalytic system Pd_2dba_3/tris(o-tolyl)phosphine [P(*o*-tolyl)$_3$] in 20% yield besides 20% DTP

© 2023 The Authors. Chemistry - A European Journal published by Wiley-VCH GmbH

15213765, 2023, 60, Downloaded from https://chemistry-europe.onlinelibrary.wiley.com/doi/10.1002/chem.202301867 by Universidad de la Rioja, Wiley Online Library on [29/11/2023]. See the Terms and Conditions (https://onlinelibrary.wiley.com/terms-and-conditions) on Wiley Online Library for rules of use; OA articles are governed by the applicable Creative Commons License

Table 1. Summary of the optimized reaction conditions of *H*-DTP **1** with 9-bromoanthracene **2b** to DTPs **3**–**5ββ**.

Entry	Pd source	Ligand	NaO*t*Bu/PivOH [equiv.]	**3** [%]	**4β** [%]	**5ββ** [%]	Total yield/β-arylation [%]
1	$Pd(OAc)_2$	Xantphos	1.5/0	63	35	0	**98**/35
2	$Pd(dba)_2$	Xantphos	1.5/0	**78**	8	0	86/8
3	$Pd(tBu_3P)_2$	BINAP	1.5/0	8	**66**	2	76/**68**
4	$Pd_2(dba)_3$	$P(tBu)_3$	4.5/1.5	0	0	**53**	53/53

Yields are given as isolated yields after separation with preparative HPLC. Reaction conditions: *H*-DTP **1** (1 equiv.), 9-bromoanthracene **2b** (2.1 equiv.), Pd source (0.1 equiv.), ligand (0.4 equiv.), toluene 110 °C, 6 d.

4β with the need of improvement. We also evaluated the reactivity of the anthracene reactant in the N-arylation reaction with $Pd(dba)_2$/Xantphos. The formation of DTP **3** with standard 9-bromoanthracene **2b** (68%) was slightly improved by 9-iodo **2c** (72%) and further by 9-chloro derivative **2a** (78%). Under these conditions, β-arylation products were formed in only minor quantities (Table S2).

The β-arylation reaction of DTP **3** to DTP **4β** with the catalytic system $Pd(tBu_3P)_2$/BINAP was further investigated by changing the base to KO*t*Bu, the solvent to m-xylene or mesitylene in order to increase the reaction temperature to 130 °C and 150 °C, respectively, or by using microwave conditions. In contrast to the N-arylation reaction, for 9-anthryl derivatives **2a** and **2c** inferior yields of DTP **4β** were obtained. Even though the reaction in mesitylene at 150 °C was less regioselective, a mixture of DTP **3**, β-arylated DTP **4β**, and twofold β,β′-diarylated DTP **5ββ** was identified in which the latter DTP **5ββ** prevailed (40%; Table S3).

In the development of direct (hetero)arylation reactions, carboxylate-assisted C–H bond functionalization became important in order to receive high-yielding reactions. In this respect, carboxylic acids were stoichiometrically added and mechanistic studies suggested that the corresponding carboxylates act as proton shuttle within the concerted metalation-deprotonation (CMD)-mechanism.[11,40] Among the various carboxylic acids,[41] in particular the addition of pivalic acid (PivOH) was prominently used for effective direct arylations of (hetero)arenes,[2,4] such as thiophenes and direct arylation polymerizations to yield conjugated (co)polymers.[7,42] The application of PivOH goes back to Fagnou et al.[43] and renders the typical use of silver(I) salts unnecessary.[10]

Therefore, we further tested PivOH as additive and optimized the reaction of *H*-DTP **1** and 9-anthryl halides **2** for β,β′-diarylated DTP **5ββ** (Table S4). By applying the catalytic system Pd_2dba_3/tBu_3P without PivOH, preferentially DTP **4β** and low yields of DTP **5ββ** were formed. However, the best results were obtained when base and PivOH were added in a ratio of 4.5/1.5 equiv. and DTP **5ββ** was selectively formed in 53% yield without any side product. Other variations, such as an increase of the amount of base/PivOH or of the halide, nor the use of other ligands did not lead to further improvements.

A summary overview of the optimized reaction conditions for the most effective preparation of DTP **3**, **4β**, and **5ββ** from *H*-DTP **1** and 9-bromoanthracene **2b** is given in Table 1. The best overall yield of 98% was achieved with the catalytic system $Pd(OAc)_2$/Xantphos, whereby N-arylation to DTP **3** (63%) prevailed over the unprecedented β-arylation to DTP **4β** (35%; entry 1). The C–N cross-coupling reaction was most efficient when the Pd source $Pd(OAc)_2$ was replaced by $Pd(dba)_2$ raising the yield of DTP **3** to 78% and simultaneously decreasing the amount of DTP **4β** (8%) (entry 2). The regioselectivity for the β-C–H activation was substantially increased when the catalytic system $Pd(tBu_3P)_2$/BINAP was used and DTP **4β** was formed in good 66% yield accompanied by low amounts (8%) of DTP **3** and twofold β,β′-diarylated DTP **5ββ** (2%; entry 3). Surprisingly, the latter sterically constrained product was selectively formed in 53% yield when the catalyst Pd_2dba_3/tBu_3P was used and PivOH added (entry 4).

Because for most catalytic systems mixtures of monoarylated **4β** and diarylated product **5ββ** in various ratios were obtained, we were interested to evaluate if diarylated DTP **5ββ** is formed from monoarylated **4β** during the reaction. A first indication came from the tracking of the product ratio over reaction time. Here, the reaction of DTP **1** and 9-bromoanthracene **2b** with the catalytic system $Pd_2(dba)_3$/BINAP in toluene at 110 °C was monitored over 10 days. Whereas in the first 3 days of reaction nearly exclusively the monoarylated DTP **4β** is formed up to around 30%, the accumulation of DTP **5ββ** starts from the third day on and in the following the product ratio then stays more or less constant (**4β**:**5ββ** ≈ 8:1; Table S5). The independent reaction of monoarylated DTP **4β** with bromide **2b** under the optimized conditions for the formation of the diarylated product (Pd_2dba_3/tBu_3P/PivOH) showed surprisingly that DTP **5ββ** could be isolated in only 10–12% yield (Scheme 2).

The structures and β-regioselectivity of the novel DTP derivatives were fully characterized and unequivocally proven by ^{1}H NMR spectroscopy (Figures S1–S11), high-resolution mass spectra (HRMS; Figures S12–S22), and single crystal X-ray structure analysis (see below). Thus for example, in the ^{1}H NMR spectra, the signal of the NH-proton is continuously high-field

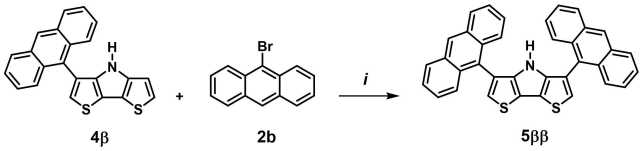

Scheme 2. Further β-arylation of mono-β-arylated DTP **4β** to DTP **5ββ**; i: Pd_2dba_3/tBu_3P/PivOH, toluene, 110 °C, 6 d.

© 2023 The Authors. Chemistry - A European Journal published by Wiley-VCH GmbH

shifted from $\delta_{NH} = 8.32$ ppm for *H*-DTP **1** to 7.81 ppm for mono-(9′-anthryl)-DTP **4β** and to 7.61 ppm for di (9′-anthryl)-DTP **5ββ**. This effect is caused by the shielding cone of the adjacent aromatic anthracene(s).

Direct arylation reactions of N-substituted DTPs 6

The tunable regioselectivity in direct arylation reactions of *H*-DTP **1** with 9-anthryl halides **2** prompted us to investigate the reaction behavior of N-substituted DTPs in order to test the selectivity of the substitution at the DTP-thiophenes. We therefore synthesized N-hexylated *Hex*-DTP **6a** from parent *H*-DTP **1** by nucleophilic substitution with hexyl iodide in a basic two-phase system according to Berlin et al.[44] and phenylated *Ph*-DTP **6b** by reacting **1** with bromobenzene in a Pd-catalyzed Buchwald–Hartwig amination (Scheme 3).[35]

We also investigated the N-substitution of β-(9′-anthryl)-substituted *H*-DTPs **4β** and **5ββ** in order to evaluate the shielding effect of the adjacent 9′-anthryl moieties. Application of the same reaction conditions to β-(9′-anthryl)-substituted DTP **4β** gave corresponding *Hex*-DTP **7aβ** and *Ph*-DTP **7bβ** in yields of 94% and 50%, respectively, indicating that single β-(9′-anthryl)-substitution does not impede substitution at the adjacent DTP nitrogen due to steric hindrance (Scheme 4).

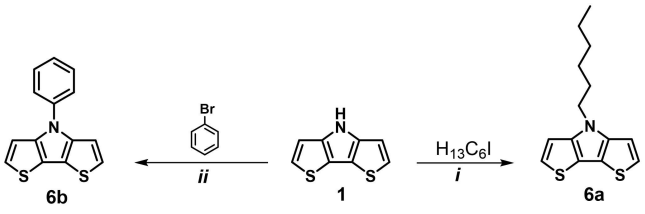

Scheme 3. N-substitution of *H*-DTP **1** to alkylated DTP **6a** and phenylated DTP **6b**. i: NaOH, toluene, 70 °C, 24 h; ii: $Pd(OAc)_2/P(tBu)_3$/NaOtBu, toluene, 110 °C, 6 d.

The use of the sterically more hindered β,β-di (9′anthryl)-substituted DTP **5ββ** in the above mentioned substitutions as well allowed for the effective alkylation with hexyl iodide and delivered *Hex*-DTP **8aββ** in excellent 95% yield. In contrast to DTP **4β** the Pd-catalyzed phenylation of DTP **5ββ** with bromobenzene unfortunately completely failed (Scheme 5).

Interestingly, in the ^{1}H NMR spectra of *Hex*-DTPs **7aβ** and **8aββ** the signals of the methylene groups are shielded by the anthracenes and high-field shifted in comparison to the corresponding protons in *Hex*-DTP **6**. The extreme is found for γ-CH_2 in *Hex*-DTPs **8aββ** with a value of $\delta = -1.07$ ppm.

The direct arylation reaction of N-substituted DTPs **6a** and **6b** with 9-bromoanthracene **2b** under the optimized pivalic acid-assisted C–H bond functionalization conditions with the catalytic system Pd_2dba_3/BINAP this time resulted in α-selective substitutions at the DTP-thiophene units. Thus, for *Hex*-DTP **6a** mixtures of 2-(9′-anthryl)-DTP **7aα** and 2,6-di-(9′-anthryl)DTP **8aαα** were obtained and after purification with preparative HPLC the pure derivatives isolated in 37% and 15% yield, respectively. A similar product ratio was obtained for the reaction of *Ph*-DTP **6b** with 9-bromoanthracene **2b** and **7bα** was isolated in 37% yield and **8bαα** in 16% yield (Scheme 6). The structures and α-regioselectivity were unambiguously proven by ^{1}H NMR spectroscopy and high resolution mass spectra (HRMS). The data was compared to samples of DTPs **8bα** and **8bαα**, which were independently synthesized by Stille-coupling reaction of 2,2'-distannylated N-phenyl-DTP[39] and 9-bromoanthracene **2b** (see the Supporting Information). One indication for the α-substitution pattern is the missing high-field shift of the hexyl-CH_2 groups in *Hex*-DTPs **7aα** and **8aαα** in ^{1}H NMR spectra. These results indicate that α-selectivity, which is highly favored in arylation reactions of other heteroacenes (see above), is obtained when the DTP nitrogen is alkylated or arylated as in **6a** or **6b**. Therefore, the unusual β-selectivity, which we obtained for the C–H activation of unsubstituted derivatives **1** and **4b**, seems to be directed by

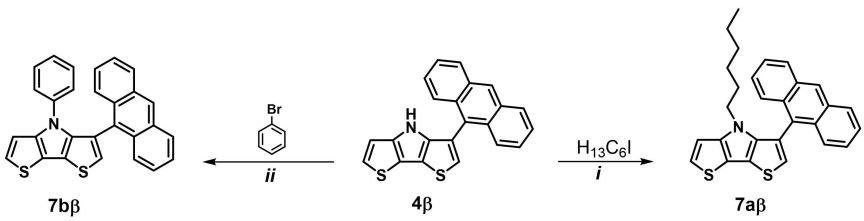

Scheme 4. N-substitution of β-arylated DTP **4β** to alkylated DTP **7aβ** and phenylated DTP **7bβ**. i: NaOH, toluene, 70 °C, 48 h; ii: $Pd(OAc)_2/tBu_3P$/NaOtBu, toluene, 110 °C, 6 d.

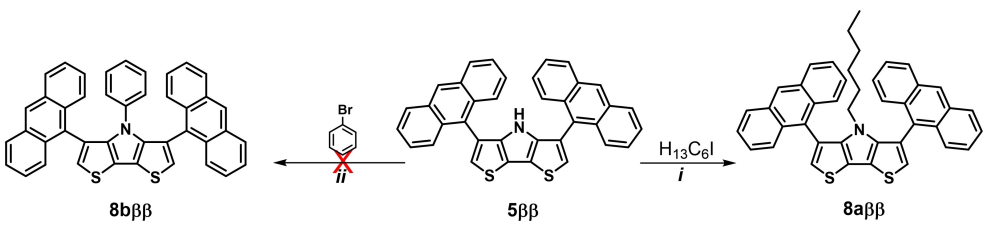

Scheme 5. N-substitution of β,β-diarylated DTP **5ββ** to alkylated DTP **8aββ**. i: NaOH, toluene, 70 °C, 24 h; ii: $Pd(OAc)_2/tBu_3P$/NaOtBu, toluene, 110 °C, 6 d.

© 2023 The Authors. Chemistry - A European Journal published by Wiley-VCH GmbH

15213765, 2023, 60, Downloaded from https://chemistry-europe.onlinelibrary.wiley.com/doi/10.1002/chem.202301867 by Universidad de la Rioja, Wiley Online Library on [29/11/2023]. See the Terms and Conditions (https://onlinelibrary.wiley.com/terms-and-conditions) on Wiley Online Library for rules of use; OA articles are governed by the applicable Creative Commons License

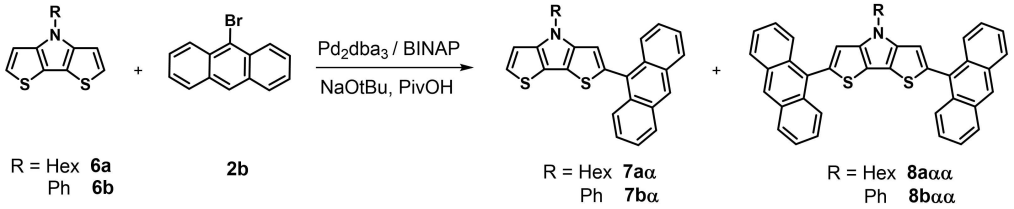

Scheme 6. α-Arylation of N-substituted DTPs **6a** and **6b** with 9-bromoanthracene **2** under Pd catalysis to give alkylated *Hex*-DTP **7aα** and **8aαα** and phenylated *Ph*-DTP **7bα** and **8bαα**, respectively.

the N–H group, whereby the mechanism is rather speculative at the moment (see below).

Single crystal X-ray structure analyses of (9′-anthryl)-DTPs 3, 4β, 5ββ, and 8aββ

Yellow single crystals suitable for X-ray structural determination of *N*-(9′-anthryl)-DTP **3** and β-arylated DTPs **4β**, **5ββ**, and **8aββ** were obtained by slow evaporation of solutions in dichloromethane (DCM) and *n*-hexane (3:7). Their molecular structures, which are in full agreement with the NMR data, were established by single crystal X-ray diffraction and their geometries are shown in Figure 1. DTP **3** crystallized in the *Pbca* space group, DTP **4** in $P2_1/c$, DTP **5** in Pn, and DTP **8** in the *C*2/*c* triclinic $P\bar{1}$ space group. The unit cells of DTPs **3**, **4**, and **8** contained eight molecules, that of **5ββ** two (Figures S23–S26). Experimental crystal data and structure refinement parameters for all structures including selected bond lengths, bond angles, and torsion angles are summarized in Tables S6–S17.[45] Bond distances and angles of the central DTP unit correspond to typical fused π-conjugated systems with reduced bond length alternation: the mean values for the bond length alternance including the terminal double bonds amounts to 0.04, excluding those bond length alternance amounts to 0.03 Å.[46,47]

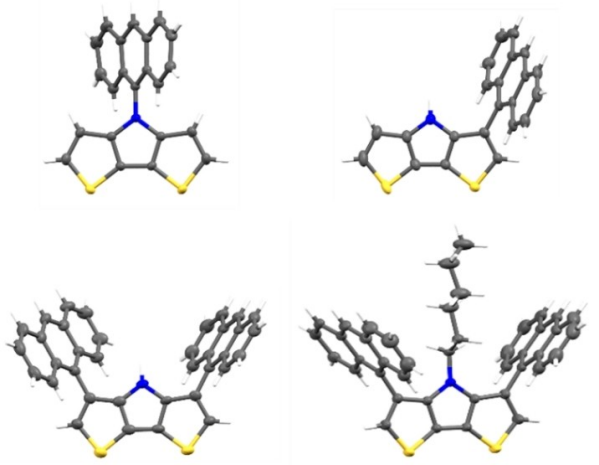

Figure 1. Single crystal X-ray structure analyses of (9′-anthryl)-DTP **3** (top, left), β-arylated DTP **4β** (top, right), β,β-diarylated DTP **5ββ** (bottom, left), and β,β-diarylated *N*-hexyl DTP **8aββ** (bottom, right). For **4β** only one (M1) of the two molecules contained in the asymmetric unit is shown. Ellipsoids for non-hydrogen atoms are set at 50% probability.

Deviations are only observed for derivative **5ββ**, whose total mean value is reduced to 0.017 Å and as a consequence almost bond length equalization (0.005 Å) is obtained for the "inner" alternating double and single bonds. Interestingly, these geometrical peculiarities have not been seen for the corresponding N-alkylated derivative **8aββ** which indicates some influence of the substituent at the DTP nitrogen on the electronic distribution in the DPT unit. In all cases, the 9′-anthryl substituents are distorted due to steric hindrance. Hence, a twist of 58° with respect to the plane of the DTP core has been determined for DTP **3** which is substantially increased compared to *Ph*-DTP **6b** (37°).[46–48] This dihedral angle is further increased to 70°/73° for the β-substituted derivatives **4β** (M1 and M2), to 58°/73° for β,β-disubstituted **5ββ**, and to 89°/81° for **8aββ** (Table 2). The almost orthogonal torsion angle of the 9′-anthryl residues with respect to the DTP plane is entirely due to repulsive interactions with the N-hexyl substituent in **8aββ**, which is squeezed in-between the two anthracene units. However, no intramolecular short contacts below the sum of the van der Waals radii of C-atoms have been found in this case.

For derivatives **3** and **5ββ**, a small (out-of-plane) bending of the anthracene units is noted which causes intramolecular short contacts between C-atoms of the anthracene and DTP unit with distances as short as 3.1 Å in the case of DTP **3** and 3.3 Å for DTP **5ββ**. Furthermore, a small but relevant helical twist of 5.4° in the plane of the N-anthracene unit is exclusively observed for DTP **3**. Finally, no packing effects are interrelated with the observed short intramolecular C–C interactions or twists for any derivative.

Quantum-chemical calculations

We carried out quantum-chemical density functional calculations (DFT) using the M062x functional and the basis 6-31G++(d,p) in order to obtain the geometry optimization of all derivatives and to analyze the impact of the substitution on the frontier molecular orbitals. Time-dependent DFT calculations (TDDFT) were performed with the CAMB3LYP functional in order to determine the character of electronic transitions. In Table 2, the frontier molecular orbital surfaces of selected DTPs with different substitution patterns are depicted.

Electron density in the lowest unoccupied molecular orbitals, LUMO and LUMO+1 (not shown) delocalizes almost exclusively on the anthracene units. Similar to other DTP analogues, the highest occupied molecular orbitals (HOMO)

© 2023 The Authors. Chemistry - A European Journal published by Wiley-VCH GmbH

15213765, 2023, 60, Downloaded from https://chemistry-europe.onlinelibrary.wiley.com/doi/10.1002/chem.202301867 by Universidad de la Rioja, Wiley Online Library on [29/11/2023]. See the Terms and Conditions (https://onlinelibrary.wiley.com/terms-and-conditions) on Wiley Online Library for rules of use; OA articles are governed by the applicable Creative Commons License

Table 2. Frontier molecular orbital surfaces of selected DTP derivatives bearing the 9′-anthryl substituents at different positions. Molecular orbital surfaces were generated by using the Gauss View 5.0 program with an isovalue of 0.02. Alkyl chains were shortened to propyl for **8aββ** and **8aαα** in order to save computational time.

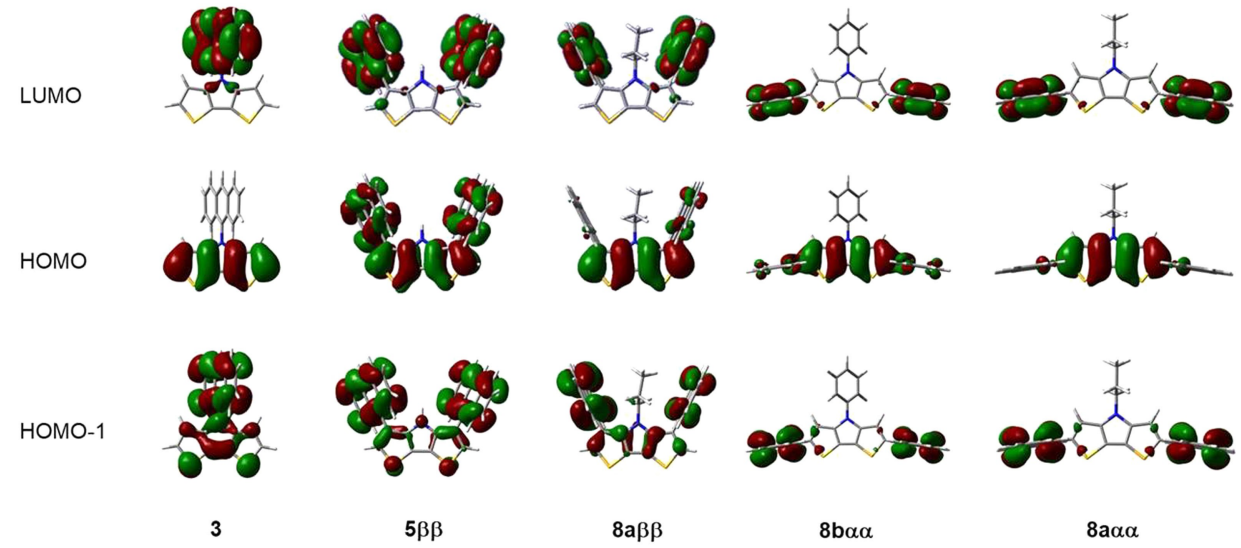

	3	**5ββ**	**8aββ**	**8bαα**	**8aαα**
Dihedral angles [a]					
Calculated	69°	64°/ 65°	88°/ 81°	89°/ 90°	88°/ 88°
X-ray analysis	58°	58°/ 73°	89°/ 81°	-	-

[a] Twist angle of the anthracene substituent with respect to the DTP-plane, calculated for the gas phase (top) and from single crystal X-ray structure analysis (bottom line).

possess a node at the nitrogen atom[48,49] and electron density is localized on the DTP unit exclusively only in the case of **3**. On the contrary the HOMO of the N-unsubstituted compounds (**5ββ** in Table 2) extends over the entire molecule. N-substitution (alkyl or phenyl) in these derivatives causes withdrawing of electron density to the DTP unit on the HOMO with minimal contribution of the anthracene units, which carry the entire electron density in the HOMO-1. In derivatives **3** and **5ββ** the HOMO-1 distributes over the entire molecule.

The calculated dihedral angles of the anthracene units in the gas phase are around 60–70° for N-substituted **3** and β,β-disubstituted **5ββ**. Interestingly, in the N-phenyl and N-hexyl α,α-disubstituted derivatives **8bαα** and **8aαα** the anthracene units are fully perpendicular with respect to the DTP-plane indicating strong mutual steric interactions.

Proposed mechanism for the direct arylation of *H*-DTP 1

The special β-selectivity for the C–H activation of the basic *H*-DTP **1** and the common α-selectivity of corresponding N-substituted DTPs **6a** and **6b** was also approached by theoretical analysis based on partial Mulliken atomic charges (MC) as a reactivity indicator of the specific interaction sites (for details, see the Supporting Information). The results of this theoretical analysis are summarized in Table S18, where local charges for the N, β-C and α-C of DTPs **1**, **6a**, and **6b** are listed. MC with full basis set (including diffuse functions) showed agreement with the experimental data. In this respect, independent of the type of substituent at the DTP nitrogen, for N-substituted DTPs **6a** and **6b** the carbon atoms at the α-position comprise more negative partial atomic charges and therefore higher reactivity. In contrast, the partial atomic charge analysis of *H*-DTP **1** showed more negative partial atomic charges at the β (−0.418) and N-position (−0.346) than at the α-position (−0.256; Figure 2). As a consequence the βC–H and N–H bonds should be more reactive for the insertion of the electropositive PdL_2-species.

For a mechanistic consideration of the unprecedented β-arylation of *H*-DTP **1**, the following observations should be taken into account. As previously reported by us, Pd-catalyzed reaction of *H*-DTP **1** with aryl and acene bromides typically resulted in direct N-arylation and C–N-coupled DTPs were isolated in mostly good yields. However, the reaction of *H*-DTP **1** with 9-bromoanthracene **2b** to DTP **3** completely failed with the standard catalytic system ($Pd(OAc)_2$/tBu_3P) used in this investigation, whereby 2-bromoanthracene reacted smoothly.[35] In contrast, the recent investigation and optimization of the catalyst now have shown that the site of arylation at the DTP core strongly varies with the steric demand of the ligand (L) chosen for the catalytic system. Thus, with sterically less demanding bidentate ligands such as Xantphos N-arylation of *H*-DTP **1** to DTP **3** widely prevails (Scheme 7, top left, Table 1). The C–N coupling should occur according to the general

© 2023 The Authors. Chemistry - A European Journal published by Wiley-VCH GmbH

15213765, 2023, 60, Downloaded from https://chemistry-europe.onlinelibrary.wiley.com/doi/10.1002/chem.202301867 by Universidad de la Rioja, Wiley Online Library on [29/11/2023]. See the Terms and Conditions (https://onlinelibrary.wiley.com/terms-and-conditions) on Wiley Online Library for rules of use; OA articles are governed by the applicable Creative Commons License

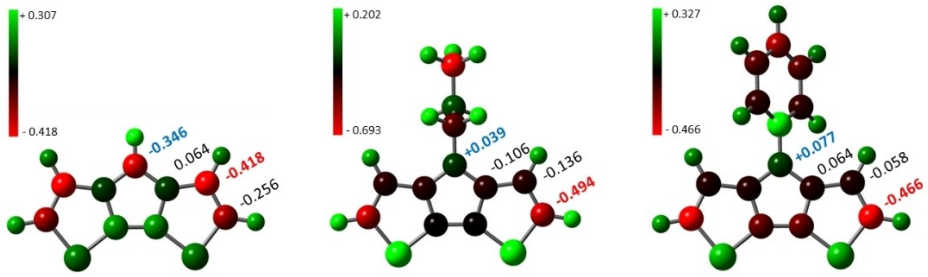

Figure 2. Color display of the partial atomic chargesobtained from the Mulliken charge population analysis for *H*-DTP **1** (left), *Hex*-DTP **6a** (middle), and *Ph*-DTP **6b** (right). To reduce computational cost, the hexyl chain in **6a** was shortened to a propyl chain.

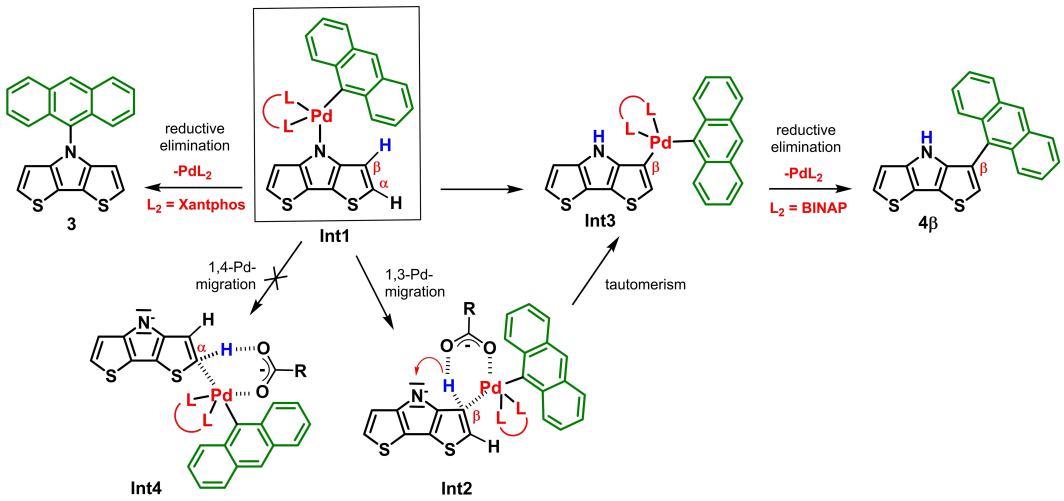

Scheme 7. Proposed catalytic C–N and C–H activation pathways for the Pd-catalyzed reaction of *H*-DTP **1** and 9-bromoanthracene **2b** via intermediate Pd complex **Int1**.

catalytic cycle of a Buchwald–Hartwig amination comprising 1) oxidative addition of PdL_2 into the aryl halogen bond, 2) transmetalation under addition of the amine, and 3) reductive elimination of the arylated amine under regeneration of the catalytically active PdL_2 fragment.[50] The change to sterically highly crowded ligands such as bidentate BINAP then quite regioselectively gave direct β-arylated C–C coupling products DTP **4β** (or **5ββ**) in good yields, whereby reductive elimination to the C–N coupled product was widely suppressed (Scheme 7, top right, Table 1).

In this respect and in analogy, slow reductive elimination from intermediate β-aryl Pd complexes have been reported by Kuwabara et al. for the C–H-activated insertion of sterically hindered 1-naphthyl into polyfluoroarenes, whereby the less hindered 2-naphthyl reacted much faster.[51] The fact, that in contrast the reaction of N-substituted DTPs **6**, which exclusively resulted in directly α-arylated products (**7α**/**8αα**, see above), suggested the specific mechanistic involvement of the NH group of *H*-DTP **1** in direct β-arylation reactions.

In the frame of the generally accepted mechanism (see above), the following mechanistic steps and intermediates, which explain the experimental observations, seem rational. Pd complex **Int1** (according to the general $L_2Pd(Ar)NR_2$ complex[49]) should be formed as central intermediate after oxidative addition of PdL_2 to the 9-bromoanthracene bond and subsequent transmetalation with *H*-DTP **1**. The β-arylation pathway might occur through 1,3-Pd migration from complex **Int1** to **Int2**, which is represented in Scheme 7 according to the concerted metalation-deprotonation (CMD) pathway for (hetero)arene C–H activation.[52] Tautomerization of the β-proton leads to Pd complex **Int3**, which subsequently undergoes intramolecular C–C bond formation and reductive elimination to β-arylated DTP **4β**. Obviously, a possible 1,4-Pd migration to α-arylated complex **Int4** seems energetically less favored and does not occur. For example, such 1,4-Pd migration and subsequent arylation via through-space C–H activation have been observed for the preparation of fused polycycles from *o*-halobiaryls by Larock et al.[53] All in all, specific regioselective βC–C coupling of *H*-DTP **1** with aryl bromides seem to function when both, sterically demanding aryl bromides, such as 9-anthryl, and sterically highly crowded phosphine ligands in PdL_2 such as bidentate BINAP are involved, so that reductive elimination from Pd complex **Int1** to the C–N coupling product is retarded and therefore 1,3-Pd migration energetically favored.[54]

In order to corroborate the postulated mechanistic pathways, DFT theoretical calculations (B3LYP/LanL2DZ) of the central Pd complexes **Int1** and **Int3** comprising both ligands,

© 2023 The Authors. Chemistry - A European Journal published by Wiley-VCH GmbH

15213765, 2023, 60, Downloaded from https://chemistry-europe.onlinelibrary.wiley.com/doi/10.1002/chem.202301867 by Universidad de la Rioja, Wiley Online Library on [29/11/2023]. See the Terms and Conditions (https://onlinelibrary.wiley.com/terms-and-conditions) on Wiley Online Library for rules of use; OA articles are governed by the applicable Creative Commons License

15213765, 2023, 60, Downloaded from https://chemistry-europe.onlinelibrary.wiley.com/doi/10.1002/chem.202301867 by Universidad de la Rioja, Wiley Online Library on [29/11/2023]. See the Terms and Conditions (https://onlinelibrary.wiley.com/terms-and-conditions) on Wiley Online Library for rules of use; OA articles are governed by the applicable Creative Commons License

Xantphos (X) and BINAP (B), have been undertaken and stabilization energies compared (Figure S27, gray bars). Thus, in the gas phase, the optimized intermediate Pd-Xantphos complex **Int1-X** is largely more stabilized by 23.2 kJ mol^{-1} than complex **Int3-X**. Interestingly, corresponding Pd-BINAP complexes **Int1-B** and **Int3-B** reveal a nearly equalized stabilization energy (2.2 kJ mol^{-1}), and explains the preferred tendency of Pd-BINAP complex **Int1** to rearrange in the discussed 1,3-Pd migration to intermediate **Int3-B**.

If one takes the dipole moment of each Pd complex into account and the fact that with toluene a nonpolar solvent is experimentally used for the reactions, the difference in stabilization energy in solution should be even larger for Pd-Xantphos complex **Int1-X** compared to **Int3-X**. This is potentially inversed in case of the Pd-BINAP complexes, where **Int3-B** becomes more stable than **Int1-B** and further underlines the experimental findings and the discussed mechanism (Figure S27, green bars).

Optical properties of (9′-anthryl)-DTPs

All DTPs were well soluble in organic solvents allowing for the investigation of their photophysical properties. UV-vis and fluorescence spectra of the (9′-anthryl)-DTPs were examined in tetrahydrofuran (THF) solutions at room temperature and compared to corresponding parent compounds *H*-DTP **1**, *Hex*-DTP **6a**, *Ph*-DTP **6b**, and anthracene (**A**). Full data for all derivatives is listed in Table 3. Electronic properties in the ground state were assessed by UV-vis absorption measurements (~10^{-5} M) and representative absorption spectra of the series DTP **3**, **4β**, and **5ββ** are depicted in Figure 3b to show the influence of the substitution position at the DTP core. Those of **8aαα** and **8aββ** are shown in Figure 3a for comparison of the α- and β-substitution pattern.

In general, all derivatives exhibited similar absorption spectra as a sum of the spectra of corresponding DTP and anthracene sub-chromophores. Thus, the low intensity band at 294–313 nm corresponds to the absorption of the DTP core. The intensive high energy band at 254–258 nm and the vibrationally resolved low energy absorption with four peaks in the regime of 330–400 nm can be assigned to π–π* excitations parallel (S_0–S_2) and perpendicular (S_0–S_1) to the molecular anthracene axis, respectively. The independent contribution of the sub-chromophores to the absorption spectra clearly indicates that no charge-transfer (CT) interactions, neither inter- nor intramolecular, are of relevance in the ground state for almost all derivatives. Exceptions to this behavior can be found in the absorption spectra of α-substituted DTPs **7bα** and **8aαα** (Figure 3a) and as well of **8bαα**. There, a less defined small intensity band at low energy can be observed independent of the concentration and in agreement with the theoretical calculations is ascribed to a CT-band. In this respect, the first electronic transition for all derivatives corresponds to a HOMO→LUMO transition with moderate intensity, as obtained from TDDFT calculations. Consequently, the low energy bands in the case of **7aβ**, **8aββ**, **7aα**, **8aαα**, and **8bαα** manifest CT-character.

The optical energy gaps were determined from the absorption onset at the lowest energy band and show the trend that for all (9′-anthryl)-substituted derivatives the gaps are significantly smaller (E_g = 3.08–2.73 eV) than for references **1**, **6a**, and **6b**. As well the α-substituted DTPs present smaller gaps than the β-substituted counterparts due to increased π-conjugation.

The molar extinction coefficients (ε) of the new DTP derivatives evidenced some trends (Table 3): for the same

Table 3. Optical data for (9′-anthryl)-DTPs **3**–**8aββ**, references *H*-DTP **1**, *Hex*-DTP **6a**, *Ph*-DTP **6b**, and anthracene **A** in THF solution.

DTP	R[a]	λ_{max}^{Abs} [nm][b]	ε [M^{-1} cm^{-1}]	λ_{max}^{Flu} [nm][c]	E_g^{opt} [eV][d]
1	H	- ‖ 294 ‖ -	22 500	–	3.95
3	A	256 ‖ 294 ‖ 368, 388	100 900	417	3.01
4β	H	256 ‖ 296 ‖ 367, 387	104 350	517	3.01
5ββ	H	254 ‖ 298 ‖ 367, 387	177 620	(377) 499	3.05
6a	Hex	- ‖ 298 ‖ -	26 600	–	3.90
6b	Ph	- ‖ 299 ‖ -	28 370	–	3.86
7aα	Hex	256 ‖ 303 ‖ 390, 414	134 520	510	2.87
7bα	Ph	256 ‖ 303 ‖ 390 (n.r.)	153 630	487	2.90
7aβ	Hex	256 ‖ 299 ‖ 368, 388	139 620	513	3.08
7bβ	Ph	258 ‖ 298 ‖ 369, 389	73 395	(376) 464	3.04
8aαα	Hex	255 ‖ 313 ‖ 389 (n.r.)[e]	203 579	(432) 492	2.73
8bαα	Ph	255 ‖ 305 ‖ 390 (n.r.)	216 193	(401) 498	2.82
8aββ	Hex	254 ‖ 303 ‖ 368, 389	202 120	(375) 499	3.08
A	H	254 ‖ 358, 375	177 340	379	3.22

[a] A = Anthracene, Hex = Hexyl, Ph=Phenyl, n.r. = not resolved. [b] The data of different electronic transitions are separated by double vertical lines (‖) and, for the longest wavelength band, the maximum (underlined) and lower energy peaks have been determined. [c] Measured in THF with an excitation wavelength of 340 nm; [d] Determined from the absorption onset at the lowest energy band. [e] Tailing to 450 nm.

© 2023 The Authors. Chemistry - A European Journal published by Wiley-VCH GmbH

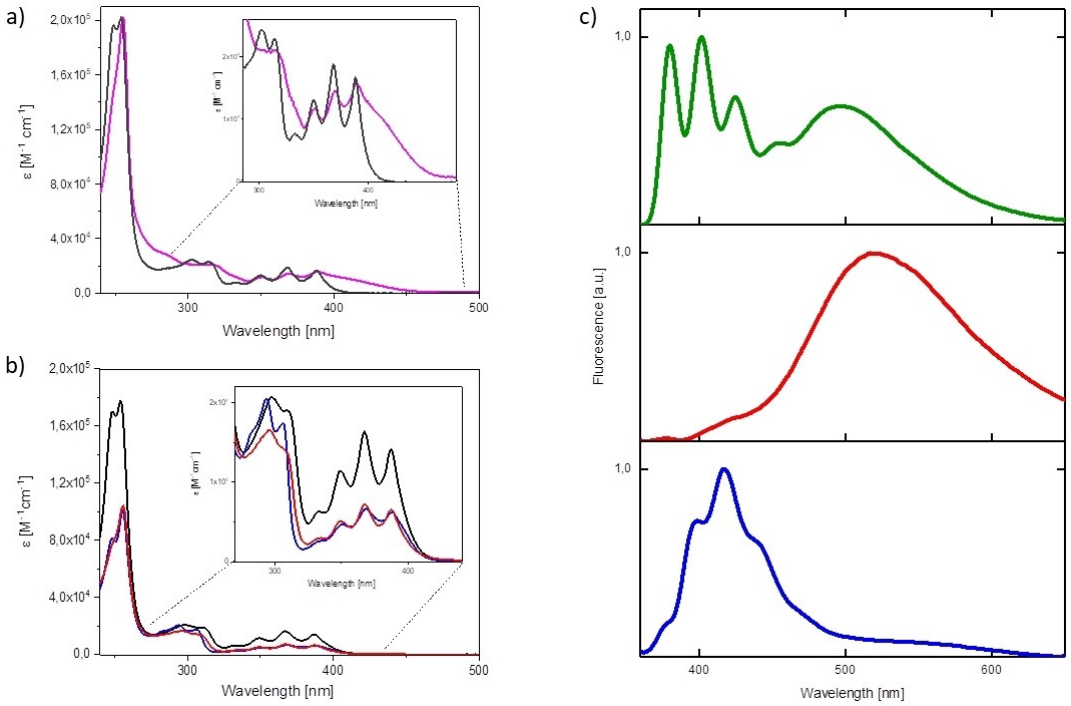

Figure 3. UV-vis spectra of THF solutions of a) di (9′-anthryl)-DTPs **8aαα** (magenta curve) and **8aββ** (dark gray) and b) (9′-anthryl)-DTPs **3** (blue curve), **4β** (red), and **5ββ** (black). c) Fluorescence spectra of (9′-anthryl)-DTPs **3** (blue curve, bottom), **4β** (red, middle), and di (9′-anthryl)-DTP **8bαα** (green, top).

substitution pattern the introduction of a second anthracene unit in the pairs **4β**/**5ββ**, **7aα**/**8aαα**, and **7bα**/**8bαα** increases ε by ≈70 000 $M^{-1}cm^{-1}$ independently of the N-substitution. N-alkylation increases ε for the pairs **4β**/**7aβ** and **5ββ**/**8aββ** which is even stronger for the N-arylated pairs **7aα**/**7bα** and **8aαα**/**8bαα**. An exception to the latter finding is represented in the case of **7aβ** and **7bβ**, where the intensity of the absorption band for the *Ph*-DTP **7bβ** substantially drops most probably due to structurally enforced π-interactions between the phenyl and anthracene units and resulting distortion which does not occur for the α-substituted *Ph*-DTP derivatives **7bα** and **8bαα**. Independent of the N-substitution, α- vs. β-functionalization barely affects the extinction coefficient ε except for **7bα**/**7bβ** due to the reasons explained above.

Fluorescence spectra were measured in THF and the data is summarized in Table 3. The fluorescence spectrum of DTP **3** (Figure 3, bottom right) shows the characteristic emission of the locally excited anthracene state (LE) at around λ_{em} = 420 nm, although the vibronic splitting of this band is notoriously less pronounced than in pristine anthracene. A closer look also evidences a non-negligible rest of emission in the region between 500–600 nm whose origin will be explained here. The fluorescence spectrum of **4β** (Figure 3, middle right) as representative of the β-substituted (9′-anthryl)-DTPs showed a broad featureless band centered at 510 nm. We can ascribe this band to the emission from an intramolecular charge transfer state (CT). Solvatochromism of the CT character of this transition has been proven and linearly correlates with the Hansen polarity parameter (Figure S28). The emission from the LE state seems to be successfully suppressed in these derivatives. The fluorescence spectra of the α-substituted (9′-anthryl)-DTPs like **8bαα** (Figure 3, top right) showed emissions with similar intensities from both excited states, the anthracene LE and the CT state. The absence of further emission bands suggests that no electronic interactions between the anthracene units are active at moderated concentrations, neither intra- nor intermolecular. All in all, Figure 4 shows a summary of ground and excited states and possible transitions between the states in absorption and emission for representatives of different substitution patterns.

Electrochemical properties of (9′-anthryl)-DTPs

In order to get information about the redox properties and energetics of the frontier orbitals, the (9′-anthryl)-DTPs were studied by cyclic voltammograms (CV) and differential pulse voltammetry (DPV) in dichloromethane (DCM) and tetrabutylammonium hexafluorophosphate (TBAHPF, 0.1 M) as electrolyte, whereby all potentials are referenced against the ferrocene/ferricenium redox couple (Fc/Fc^+) and determined from corresponding DPVs (Table 4).

All derivatives showed two irreversible oxidation waves due to follow-up reactions of the charged species and formation of higher-molecular-weight oligomers or polymers (see above).[37,55] In Figure 5, representative CVs for di (9′-anthryl)-substituted DTP **8aββ** (left) and **8aαα** (right) are depicted. Here, the first (irreversible) redox process, which is addressed to the oxidation of the DTP-subunit, is at lower potential for the α,α-disubstituted derivative **8aαα** (E_p^{Ox1} = 0.38 V) than for corre-

© 2023 The Authors. Chemistry - A European Journal published by Wiley-VCH GmbH

15213765, 2023, 60, Downloaded from https://chemistry-europe.onlinelibrary.wiley.com/doi/10.1002/chem.202301867 by Universidad de la Rioja, Wiley Online Library on [29/11/2023]. See the Terms and Conditions (https://onlinelibrary.wiley.com/terms-and-conditions) on Wiley Online Library for rules of use; OA articles are governed by the applicable Creative Commons License

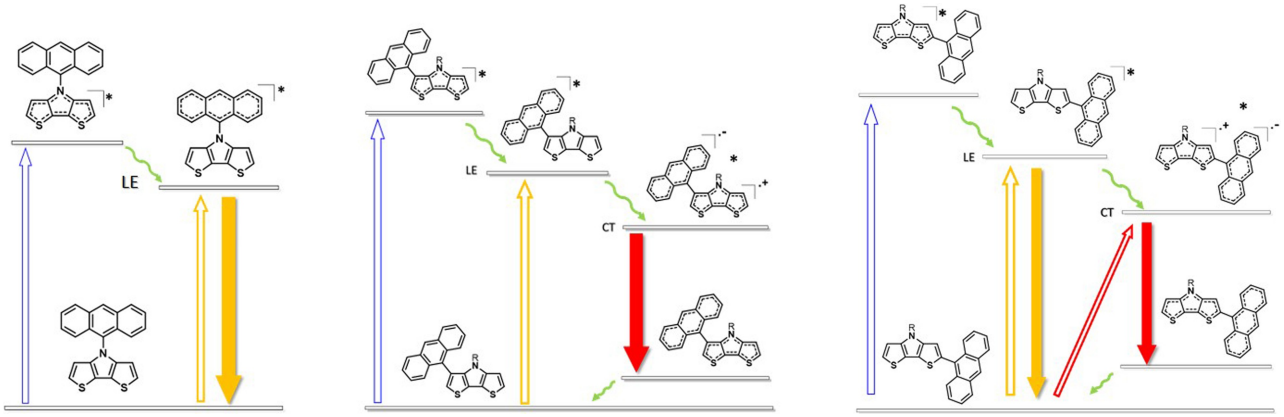

Figure 4. Simplified two and full three-excited state models for the N-, β-, and α-substituted DTP derivatives (**3** (left), **4β** (middle), and **7aα** (right) and observed transitions (absorption transitions white-filled blue and orange arrows, emission from LE and CT states, plain orange and red arrows, respectively). Green arrows indicate nonradiative deactivation pathways between states.

Table 4. Redox data of (9′-anthryl)-DTPs **3**–**8aββ** and references *H*-DTP **1**, *Hex*-DTP **6a**, *Ph*-DTP **6b**, and anthracene **A** deduced from differential pulse voltammetry (DPV) measured in dichloromethane at RT.

DTP	R	E_p^{Ox1} [V]	E_p^{Ox2} [V]	E_{onset} [V]	E_{HOMO} [eV][a]	E_{LUMO} [eV][b]	E_g^{CV} [eV][c]
1	H	0.49	–	0.39	−5.49	−1.54	3.95
3	H	0.52	1.21	0.44	−5.54	−2.53	3.01
4β	H	0.62	1.15	0.52	−5.62	−2.61	3.01
5ββ	H	0.63	1.18	0.54	−5.64	−2.59	3.05
6a	Hex	0.46[d]	–	0.40	−5.50	−1.60	3.90
6b	Ph	0.55[d]	–	0.50	−5.60	−1.74	3.86
7aα	Hex	0.43	1.05	0.37	−5.47	−2.60	2.87
7aβ	Hex	0.49	1.14	0.47	−5.57	−2.49	3.08
7bα	Ph	0.48	1.02	0.43	−5.53	−2.63	2.90
7bβ	Ph	0.58	1.10	0.54	−5.54	−2.50	3.04
8aαα	Hex	0.38	0.96	0.33	−5.43	−2.70	2.73
8aββ	Hex	0.57	0.99	0.52	−5.62	−2.54	3.08
8bαα	Ph	0.44	0.97	0.38	−5.48	−2.66	2.82
A	H	0.86		0.77	−5.80	−2.58	3.22

[a] Determined from the onset of the first oxidation wave; [b] Determined by taking the optical gap into account ($E_{LUMO} = E_{HOMO} - E_g^{opt}$); [c] $E_g^{CV} = E_{HOMO} - E_{LUMO}$; [d] Potential derived from cyclic voltammetry, Ref. [48].

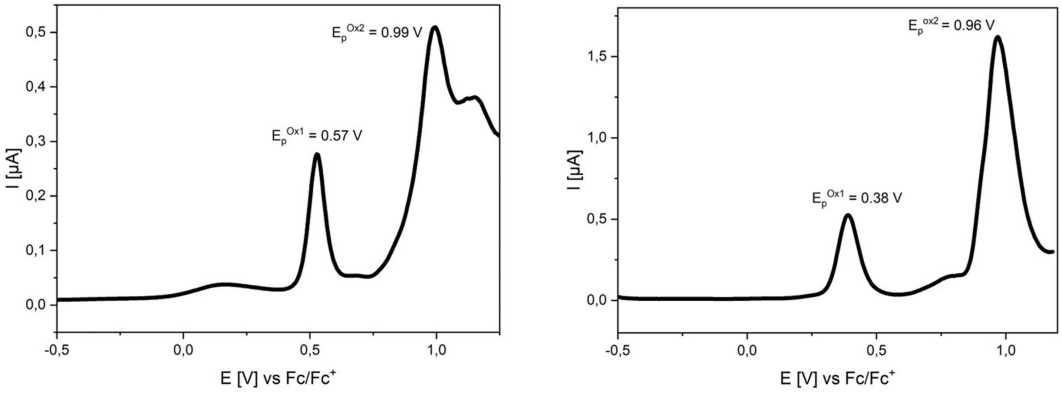

Figure 5. DPVs of di (9′-anthryl)-substituted DTP **8aββ** (left) and **8aαα** (right) in dichloromethane/TBAHPF (0.1 M), 100 mV s^{-1}, RT.

© 2023 The Authors. Chemistry - A European Journal published by Wiley-VCH GmbH

15213765, 2023, 60, Downloaded from https://chemistry-europe.onlinelibrary.wiley.com/doi/10.1002/chem.202301867 by Universidad de la Rioja, Wiley Online Library on [29/11/2023]. See the Terms and Conditions (https://onlinelibrary.wiley.com/terms-and-conditions) on Wiley Online Library for rules of use; OA articles are governed by the applicable Creative Commons License

sponding β,β derivative **8aββ** ($E_p^{Ox1} = 0.52$ V) due to the increased π-conjugation via the α-positions. The second (irreversible) oxidation, however, is affiliated with anthracene oxidation and rather invariant for both DTPs (E_p^{Ox1} = 0.96-0.99 V). This consequence of the substitution pattern on the redox potentials is also evident for the pairs **7aα/7aβ** and **7bα/7bβ** and follows the trend already seen for the optical properties.

Rather subtle differences can be noted in the series of N-substituted **3**, β-substituted DTPs **4β**, and β,β′-**5ββ** where E_p^{Ox1} only varies from 0.52 to 0.63 V and E_p^{Ox2} from 1.15 to 1.21 V. As a general trend, the redox potentials of the DTP/anthracene hybrids were typically found at more positive potentials compared to those of the individual parent subunits, DTP **1**, *Hex*-DTP **6a**, *Ph*-DTP **6b**, and anthracene **A**.

From the onset of the first oxidation peak, HOMO energy values and with the aid of the optical energy gap corresponding LUMO energies were determined. Hence, the resulting electrochemical energy gap is smallest for α-substituted DTP **8aαα** ($E_g^{CV} = 2.73$ eV) and largest for β-disubstituted DTPs **7aβ** and **8aββ** (both, $E_g^{CV} = 3.08$ eV) due to the different π-conjugation.

Oxidative polymerization of selected (9′-anthryl)-DTP derivatives

DTPs have been frequently polymerized to poly(dithienopyrroles), p(DTP)s, or were applied as building block in a manifold of co-polymers designed for application in organic solar cells.[48] P(DTP)s can be best prepared by chemical or electrochemical oxidative polymerization due to facile coupling of the formed DTP-radical cations via the reactive α-positions. The resulting conjugated polymers typically show high conjugation length ($\lambda_{max} \approx 550$ nm) and can be reversibly oxidized. Larger or bulky alkyl substituents at the DTP nitrogen renders them soluble in organic solvents allowing for structural characterization.[37,48]

In this respect, we investigated the electrochemical polymerization of differently substituted DTP monomers with open α-positions **3**, **4β**, **7aβ**, and **8aββ** in acetonitrile/TBAHPF (0.1 M) as electrolyte by multiple potentiodynamic cycling. Thus, under comparable conditions corresponding polymers were formed, whereby only **P4β** adhered as dark blue film on the platinum working electrode and was subsequently characterized in an electrolyte free of monomer (Scheme 8). Polymers **P3**, **P7aβ**, and **P8aββ** were soluble in the electrolyte and diffused away from the working electrode as a dark-blue haze.

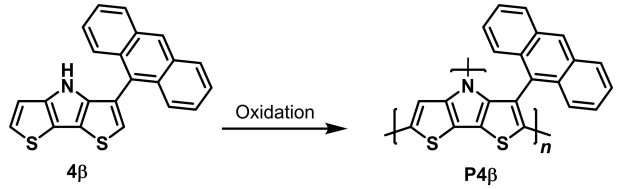

Scheme 8. Electropolymerization of β-substituted DTPs **4β** to the corresponding p(DTP) **P4β**.

The evolution of polymer formation for DTP **4β** is depicted in Figure 6. The first scan, which corresponds to the monomer characterization ($E_p^{Ox} = 0.62$ V), is plotted in red, the successive multiple scans, in which new redox waves with continuously increasing current appeared at lower potentials are represented in black (dotted). Finally, the electrochemical response and CV of the adhering DTP-**P4β** film is overlaid as black curve. Here, we note a nearly symmetrically shaped redox wave, which is quite typical for conducting polymers, exhibiting an oxidation peak potential of $E_p^{Ox} = 0.05$ V and corresponding reduction peak potential of $E_p^{Red} = 0.03$ V. The evolution of the polymer CV in dependence of the scan rate and the linear plot of the anodic and cathodic peak currents versus the scan rate indicates a well adhering polymer film on the working electrode (Figure S28). As the form and shape of CVs of conducting polymers might vary depending on their (sub)structure,[48,55] the better meaningful potential onset was determined to $E_{onset} \approx -0.25$ V indicating the ease of oxidation of the polymer and the transition from the semiconducting to the conducting state. In that respect, the potential onset of **P4β** films was determined to about 0.3 V more positive potential compared to **P1** and **P6a** which is due to a somewhat lower conjugation in the DTP unit and well correlates to the onset potential of poly(ββ′-dimethyl-DTP).[37] We address this effect to distortions of DTP units in the polymeric main chain triggered by the steric demand of the β-(9′-anthryl) substituents. Correspondingly, the HOMO energy of **P4β** which was determined from the onset potential, is stabilized and lowered from around −4.5 eV for parent p(DTP)s **P1** and **P6a**[48] to ≈ −4.95 eV. Finally, we investigated the film stability by measuring 30 cycles in a defined potential window in order to avoid over-oxidation of the polymer. The loss of electroactivity and exchange of charges resulted to only 1.5% indicating a highly stable polymer in both states (Figure S29).

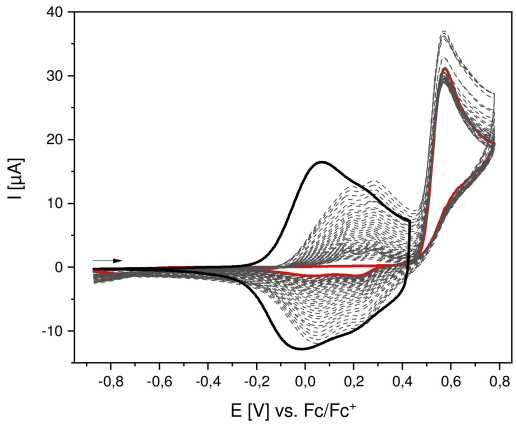

Figure 6. Potentiodynamic polymerization of the DTP monomer **4β** in acetonitrile ($c \approx 0.01$ M), TBAHFP (0.1 M), 100 mV s^{-1}, RT). The first scan (red) characterizes the oxidation of the monomer, scans 2–40 (dotted lines) reflect the continuous growing of the polymer on the working electrode. The CV (2nd scan) of the obtained polymer films **P4β** in an electrolyte free of monomer (ACN/TBAHFP (0.1 M), 100 mV s^{-1}, RT) is shown as a black, bold curve.

© 2023 The Authors. Chemistry - A European Journal published by Wiley-VCH GmbH

15213765, 2023, 60, Downloaded from https://chemistry-europe.onlinelibrary.wiley.com/doi/10.1002/chem.202301867 by Universidad de la Rioja, Wiley Online Library on [29/11/2023]. See the Terms and Conditions (https://onlinelibrary.wiley.com/terms-and-conditions) on Wiley Online Library for rules of use; OA articles are governed by the applicable Creative Commons License

Conclusions

In summary, we have presented novel, regioselectively controlled direct arylations of dithieno[3,2-*b*:2,3′-*d*]pyrroles (DTP) **1** with 9-anthryl halides **2**. Depending on the choice of the catalytic system consisting of Pd source, ligand, and additives, either efficient N-arylation or unprecedented β-substitution of the DTP core by selective C–H activation was achieved. For N-substituted DTPs **6**, regioselective carboxylate-assisted arylation of the α-position(s) was provided. Overall, series of functionalized DTPs with N-, very rarely reported β and β,β′-di (9′-anthryl) and as well α and α,α′-di (9′-anthryl) scaffolds were obtained with mostly good to excellent yields. The novel DTP derivatives **3**–**8** were fully structurally characterized and single-crystal X-ray structure analysis combined with quantum chemical calculations gave insight into the influence of the substitution position on the geometric and electronic structure. The specific regioselective βC–C coupling of *H*-DTP **1** with aryl bromides functions well when both sterically very demanding phosphine ligands, such as BINAP or tBu$_3$P, in the active PdL$_2$ catalyst on one side and highly crowded aryl bromides, such as 9-bromoanthracene, on the other side are involved. We rationalize this result as reductive elimination from an intermediate Pd complex (**Int1**), in which the ArPdL$_2$ fragment is coordinated to the DTP nitrogen, to the typical C–N coupling product **3** is retarded and therefore an energetically favored 1,3-Pd migration and insertion into the βC–H of the DTP unit takes place.

Investigation of optical and redox properties of the various (9′-anthryl)-DTPs led to valuable structure–property relationships showing that, in contrast to β-substituted DTPs, the extension of the DTP unit via the α-positions results in more extended π-conjugation, that is, red-shifted absorptions and lower oxidation potentials. As an example of application, electrochemical polymerization of (9′-anthryl)-DTP **4β** was demonstrated to lead to a corresponding electrochemically very stable conducting polymer. Further investigation of the scope and limitation of this novel and quite special C–H-activated direct arylation method with respect to other heteroaromatic substrates and other sterically hindered arene halogenides is ongoing in our lab.

Experimental Section

General procedure for the reaction of *H*-DTP 1 and 9-anthryl halides 2 to arylated DTPs 3, 4β, and 5ββ: A suspension of 1 equiv. of *H*-DTP **1**, 2.1 equiv. 9-anthryl halide **2**, 0.1 equiv. of palladium catalyst, 0.4 equiv. of ligand were placed in a screwcap vial and dried in vacuo for several hours. Afterwards, degassed toluene (1.5 mL) and solid NaOtBu as well as 1.5 equiv. of pivalic acid for the reaction of **5ββ** were added. The closed screwcap vial was then heated to 110 °C for 6 d. Afterwards the crude reaction mixture was filtered through a silica plug. The plug was thoroughly washed with DCM. After removal of the solvent by rotary evaporation, the crude product was purified by preparatory HPLC to isolate the corresponding (9′-anthryl)-DTPs **3**, **4β**, and **5ββ** as light yellow solids.

4-(9′-Anthracenyl)-4*H*-dithieno[3,2-*b*:2′,3′-*d*]pyrrole (3): Pd(dba)$_2$ (10 mg, 0.01 mmol), Xantphos (26 mg, 0.04 mmol), NaOtBu (16 mg, 0.17 mmol). HPLC: *n*-hexane/DCM, gradient 80:20 to 20:80 (16 min). DTP **3** was obtained (110 mg, 0.42 mmol, 77%). Mp 250–251 °C; ^{1}H NMR (CDCl$_3$, 400 MHz): δ = 8.64 (s, 1H, Anth-H_{10}), 8.13 (ddt, J = 8.4, 1.1, 0.6 Hz, 2H, Anth-*H*), 7.50 (ddt, J = 14.2, 7.8, 1.1 Hz, 4H, Anth-*H*), 7.43-7.33 (m, 2H, Anth-*H*), 7.08 (d, J = 5.3 Hz, 2H, Th-H_α), 6.49 (d, J = 5.3 Hz, 2H, Th-H_β) ppm; ^{13}C NMR (CDCl$_3$, 101 MHz): δ = 147.3, 131.9, 130.6, 129.1, 128.7, 128.1, 127.2, 125.9, 123.6, 123.4, 116.0, 112.4 ppm.; HRMS (MALDI): m/z = [M^+] $C_{22}H_{13}NS_2$: calc. 355.0485, found 355.0483, δm/m = 0.3 ppm.

3-(9′-Anthracenyl)-4*H*-dithieno[3,2-*b*:2′,3′-*d*]pyrrole (4β): Pd(P(tBu)$_3$)$_2$ (14 mg, 0.01 mmol), BINAP (28 mg, 0.04 mmol), NaOtBu (16 mg, 0.17 mmol). HPLC: *n*-hexane/DCM gradient 80:20 to 20:80 over 16 min. DTP **4β** was obtained (26 mg, 0.07 mmol, 66%). Mp 221–223 °C; ^{1}H NMR (CDCl$_3$, 400 MHz): δ = 8.54 (s, 1H, Anth-H_{10}), 8.06 (dt, J = 8.6, 0.7 Hz, 2H, Anth-*H*), 7.89 (dd, J = 8.9, 1.1 Hz, 2H, Anth-*H*), 7.81 (s, 1H, N-*H*), 7.48 (ddd, J = 8.3, 6.6, 1.2 Hz, 2H, Anth-*H*), 7.36 (ddd, J = 8.8, 6.5, 1.3 Hz, 2H, Anth-*H*), 7.24 (s, 1H, Th-H_α), 7.12 (d, J = 5.2 Hz, 1H, Th-H_α), 6.80 (d, J = 5.3 Hz, 1H, Th-H_β) ppm; ^{13}C NMR (CDCl$_3$, 101 MHz): δ = 144.4, 143.4, 131.6, 130.9, 128.8, 128.7, 127.6, 126.6, 126.2, 125. 6, 123.6, 123.5, 123.2, 116.8, 116.1, 112.3 ppm; HRMS (APCI): m/z [M + H]$^+$, calc. for $C_{22}H_{13}NS_2$, 356.0562, found 356.0569, δm/m = 1.7 ppm.

3,3′-Di (9′-anthracenyl)-4*H*-dithieno[3,2-*b*:2′,3′-*d*]pyrrole (5ββ): Pd$_2$(dba)$_3$ (10 mg, 0.01 mmol), tBu$_3$P (9 mg, 0.044 mmol), NaOtBu (48 mg, 0.50 mmol, 4.5 equiv.) and PivOH (17 mg, 0.17 mmol, 1.5 equiv.). HPLC: *n*-hexane/DCM, gradient 80:20 to 20:80 (16 min). **5ββ** was obtained (31 mg, 0.06 mmol, 53%). Mp 364–365 °C; ^{1}H NMR (CDCl$_3$, 400 MHz): δ = 8.41 (d, J = 3.5 Hz, 2H, Anth-H_{10}), 7.98-7.90 (m, 4H, Anth-*H*), 7.90-7.80 (m, 4H, Anth-*H*), 7.49 (s, 1H, N-*H*), 7.38 (ddt, J = 9.8, 4.7, 2.3 Hz, 4H, Anth-*H*), 7.31 (ddd, J = 8.9, 6.5, 1.4 Hz, 4H, Anth-*H*), 7.26 (s, 2H, Th-H_α) ppm. ^{13}C NMR (CDCl$_3$, 101 MHz): δ = 144.7, 131.9, 131.1, 128.9, 128.9, 127.9, 126.7, 126.4, 125.8, 124.1, 124.0, 116.8. ppm; HRMS (MALDI): m/z [M + H] $C_{36}H_{21}NS_2$: calc. 531.1110, found 531.1099, δm/m = 2.03 ppm.

General procedure for the reaction of Hex-DTP 6a and Ph-DTP 6b with 9-bromoanthracene 2b to arylated DTPs 7aα, 8aαα, and 7bα, 8bαα: A suspension of 1 equiv. of N-substituted DTP **6a**/**6b**, 2.1 equiv. 9-bromoanthracene **2b**, 0.1 equiv. of Pd[P(tBu)$_3$]$_2$, 0.4 equiv. of BINAP, and 1 equiv. of pivalic acid were placed in a screwcap vial and dried in vacuo for several hours. Afterwards, degassed toluene (6 mL) and 3 equiv. of solid NaOtBu were added. The closed screwcap vial was then heated to 110 °C for 7 d. Afterwards the crude reaction mixture was filtered through a silica plug. The plug was thoroughly washed with DCM. After removal of the solvent by rotary evaporation, the crude product was purified by column chromatography to isolate DTPs **7aα**/**8aαα** in a first fraction and DTPs **7bα**/**8bαα** in a second fraction as light yellow solids.

2-(9′-Anthracenyl)-4-hexyl-4*H*-dithieno[3,2-*b*:2′,3′-*d*]pyrrole (7aα): 4-Hexyl-DTP **6a** (100 mg, 0.38 mol), 9-bromoanthracene **2b** (204 mg, 0.80 mmol), Pd(P(tBu)$_3$)$_2$ (19.4 mg, 0.04 mmol), BINAP (94.5 mg, 0.15 mmol), and pivalic acid (38,7 mg, 0.38 mmol). Afterwards degassed toluene (6 mL) and NaOtBu (109.4 mg, 1.14 mmol) were added. Column chromatography: SiO$_2$, PE/DCM (85:15). **7aα** was obtained in the first fraction (62 mg, 0.14 mmol, 37%). Mp 129–132 °C, ^{1}H NMR (CD$_2$Cl$_2$, 400 MHz): δ = 8.57 (s, 1H, Anth-$H_{10'}$), 8.05 (dd, J = 14.1, 8.6 Hz, 4H, Anth-*H*), 7.53–7.39 (m, 4H, Anth-*H*), 7.21 (d, J = 5.4 Hz, 1H, Th-H$_6$), 7.18 (s, 1H, Th-H$_3$), 7.13 (d, J = 5.4 Hz, 1H, Th-H$_5$), 4.29 (t, J = 7.0 Hz, 2H,CH$_2$-H_α), 1.94 (p, J = 7.1 Hz, 2H, CH$_2$-H_β), 1.31–1.25 (m, 6H, CH$_2$-$H_{\gamma,\delta,\varepsilon}$), 0.85 (t, J = 7.1 Hz, 3H, CH$_3$-H_ζ) ppm.^{13}C NMR (CD$_2$Cl$_2$, 101 MHz): δ = 145.2, 144.8, 136.4, 132.7, 131.8, 130.0, 128.8, 128.6, 127.2, 126.5, 125.9, 123.5, 116.0, 115.2, 114.5, 111.8, 48.1, 32.0, 31.0, 27.3, 23.1, 14.3 ppm. HRMS (MALDI): m/z [M + H] $C_{28}H_{25}NS_2$: calc. 439.1428, found 439.1421, δm/m = 1.7 ppm.

© 2023 The Authors. Chemistry - A European Journal published by Wiley-VCH GmbH

15213765, 2023, 60, Downloaded from https://chemistry-europe.onlinelibrary.wiley.com/doi/10.1002/chem.202301867 by Universidad de la Rioja, Wiley Online Library on [29/11/2023]. See the Terms and Conditions (https://onlinelibrary.wiley.com/terms-and-conditions) on Wiley Online Library for rules of use; OA articles are governed by the applicable Creative Commons License

2,2'-Di (9'-anthracenyl)-4-hexyl-4*H*-dithieno[3,2-*b*:2',3'-*d*]pyrrole (8 aαα) was isolated in the second fraction (36 mg, 0.06 mmol, 15%). Mp 174–176 °C, ^{1}H NMR (CD_2Cl_2, 400 MHz): δ = 8.51 (s, 2H, Anth-$H_{10'}$), 8.01 (dd, J = 8.1, 4.0 Hz, 8H, Anth-*H*), 7.46–7.38 (m, 8H, Anth-*H*), 7.18 (s, 2H, Th-H_3), 4.29 (t, J = 7.0 Hz, 2H, CH_2-H_α), 1.93 (p, J = 7.1 Hz, 2H, CH_2-H_β), 1.36 (td, J = 8.8, 8.1, 5.4 Hz, 2H, CH_2-H_γ), 0.78 (dt, J = 14.0, 6.5 Hz, 7H, CH_2-$H_{\delta,\varepsilon}$, CH_3-H_ζ) ppm. NMR (CD_2Cl_2, 101 MHz): δ = 143.9, 136.1, 132.1, 131.2, 129.5, 128.3, 128.1, 126.7, 126.0, 125.3, 115.7, 114.0, 47.7, 31.4, 30.5, 26.8, 22.6, 13.7 ppm. HRMS (MALDI): *m/z* [*M*+ H] $C_{42}H_{33}NS_2$: calc. 615.2054, found 615.2048, δm/m = 1.1 ppm.

2-(9'-Anthracenyl)-4-phenyl-4*H*-dithieno[3,2-*b*:2',3'-*d*]pyrrole (7 bα). 4-Phenyl-DTP **6 b** (100 mg, 0.39 mol), 9-bromoanthracene **2 b** (211 mg, 0.82 mmol), Pd[P(*t*Bu)$_3$]$_2$ (20.0 mg, 0.04 mmol), BINAP (97.5 mg, 0.16 mmol) and pivalic acid (39,9 mg, 0.39 mmol). Column chromatography: SiO_2, PE/DCM (85 : 15) to give DTP **7bα** in a first fraction (63 mg, 0.14 mmol, 37%). Mp 119–121 °C, ^{1}H NMR (CD_2Cl_2, 400 MHz): δ = 8.49 (s, 1H, Anth-H_{10}), 7.97 (t, J = 9.0 Hz, 4H, Anth-*H*), 7.63 (dd, J = 8.1, 1.6 Hz, 2H, Ph-*H*), 7.48-7.33 (m, 6H, Anth-*H*, PH-*H*), 7.26 (d, J = 3.0 Hz, 1H, Th-H_3), 7.25–7.22 (m, 1H, Ph-H_p), 7.22-7.19 (m, 2H, Th-$H_{2',3'}$) ppm. ^{13}C NMR (CD_2Cl_2, 101 MHz): δ = 144.6, 144.1, 143.8, 140.4, 137.3, 132.6, 131.7, 130.4, 129.6, 128.8, 128.8, 127.1, 126.6, 125.9, 124.3, 124.1, 123.1, 118.4, 117.7, 115.6, 112.9, 112.9 ppm. HRMS (MALDI): *m/z* [*M*+H] $C_{28}H_{17}NS_2$: calc.: 431.0802, found: 431.0790, δm/m = 2.8 ppm.

2,2'-Di-(9'-anthracenyl)-4-phenyl-4H-dithieno[3,2-*b*:2',3'-*d*]pyrrole (8 bαα) was isolated in a second fraction (37 mg, 0.06 mmol, 16%). Mp 192–194 °C, ^{1}H NMR (CD_2Cl_2, 400 MHz): δ = 8.60 (s, 2H, Anth-H_{10}), 8.15-8.03 (m, 8H, Anth-H), 7.84–7.76 (m, 2H, Ph–H), 7.50 (dddd, J = 15.9, 8.1, 6.5, 1.4 Hz, 10H, Anth-H, Ph–H), 7.45 (s, 2H, Th-$H_{3,3'}$), 7.31–7.27 (m, 1H, Ph-H_p) ppm. ^{13}C NMR (CD_2Cl_2, 101 MHz): δ = 142.7, 137.0, 132.1, 131.2, 129.9, 129.8, 129.0, 128.3, 128.1, 126.6, 126.5, 126.1, 125.4, 125.3, 122.5, 115.1 ppm. HRMS (MALDI): *m/z* [*M*+ H] $C_{42}H_{25}NS_2$: calc. 607.1428, found 607.1414, δm/m = 2.3 ppm.

Deposition Numbers 2266784 (for DTP **3**), 2266773 (for DTP **4 β**), 2266437 (for DTP **5 ββ**), 2266332 (for DTP **8 aββ**)) contain the supplementary crystallographic data for this paper. These data are provided free of charge by the joint Cambridge Crystallographic Data Centre and Fachinformationszentrum Karlsruhe Access Structures service.

Supporting Information

Materials and instrumentation, synthetic details, ^{1}H,^{13}C NMR spectra, HRMS spectra, single-crystal X-ray structure analysis, optical spectroscopy, electrochemistry. The authors have cited additional references within the Supporting Information.[56–65]

Acknowledgements

We thank L. Kroner, Inorganic Chemistry I, University of Ulm, for X-ray diffraction measurements and Dr. Markus Wunderlin, Service Center Mass Spectrometry, University of Ulm, for numerous high-resolution mass spectra. The authors acknowledge support by the state of Baden-Württemberg through bwHPC and the German Research Foundation (DFG) through grant no INST 40/575-1 FUGG (JUSTUS 2 cluster). Open access funding enabled and organized by Projekt DEAL. J.M. thanks the Universidad de La Rioja for the financial support (EICOD22/09). Open Access funding enabled and organized by Projekt DEAL.

Conflict of Interests

The authors declare no conflict of interest.

Data Availability Statement

The data that support the findings of this study are available from the corresponding author upon reasonable request.

Keywords: C–H activation · direct arylation · dithienopyrroles · optoelectronic properties · quantum chemical calculations

[1] P. Bujak, I. Kulszewicz-Bajer, M. Zagorska, V. Maurel, I. Wielgus, A. Pron, *Chem. Soc. Rev.* **2013**, *42*, 8895–8999.
[2] L. G. Mercier, M. Leclerc, *Acc. Chem. Res.* **2013**, *46*, 1597–1605.
[3] S. I. Gorelsky, *Coord. Chem. Rev.* **2013**, *257*, 153–164.
[4] Y. Segawa, T. Maekawa, K. Itami, *Angew. Chem. Int. Ed.* **2015**, *54*, 66–81.
[5] N. S. Gobalasingham, B. C. Thompson, *Progr. Polym. Sci.* **2018**, *83*, 135–201.
[6] S. Bensaid, J. Roger, K. Beydoun, D. Roy, H. Doucet, *Synth. Commun.* **2011**, *41*, 3524–3531.
[7] F. Lombeck, F. Marx, K. Strassel, S. Kunz, C. Lienert, H. Komber, R. Friend, M. Sommer, *Polym. Chem.* **2017**, *8*, 4738–4745.
[8] T. Bura, S. Beaupré, M.-A. Légaré, J. Quinn, E. Rochette, J. T. Blaskovits, F.-G. Fontaine, A. Pron, Y. Li, M. Leclerc, *Chem. Sci.* **2017**, *8*, 3913–3925.
[9] J. T. Blaskovits, P. A. Johnson, M. Leclerc, *Macromolecules* **2018**, *51*, 8100–8113.
[10] a) S. Yanagisawa, K. Ueda, H. Sekizawa, K. Itami, *J. Am. Chem. Soc.* **2009**, *131*, 14622–14623; b) K. Ueda, S. Yanagisawa, J. Yamaguchi, K. Itami, *Angew. Chem.* **2010**, *122*, 9130–9133.
[11] S.-Y. Tang, Q.-X. Guo, Y. Fu, *Chem. Eur. J.* **2011**, *17*, 13866–13876.
[12] I. Schnapperelle, S. Breitenlechner, T. Bach, *Org. Lett.* **2011**, *13*, 3640–3643.
[13] a) S. Kirchberg, S. Tani, K. Ueda, J. Yamaguchi, A. Studer, K. Itami, *Angew. Chem. Int. Ed.* **2011**, *50*, 2387–2391; b) K. Yamaguchi, J. Yamaguchi, A. Studer, K. Itami, *Chem. Sci.* **2012**, *3*, 2165–2169; c) K. Yamaguchi, H. Kondo, J. Yamaguchi, K. Itami, *Chem. Sci.* **2013**, *4*, 3753–3757.
[14] K. Funaki, T. Sato, S. Oi, *Org. Lett.* **2012**, *14*, 6186–6189.
[15] a) K. Yuan, H. Doucet, *Chem. Sci.* **2014**, *5*, 392–396; b) W. Hagui, H. Doucet, J.-F. Soulé, *Chem* **2019**, *5*, 2006–2078; c) W. Hagui, N. Besbes, E. Srasra, T. Roisnel, J.-F. Soulé, H. Doucet, *Org. Lett.* **2016**, *18*, 4182–4185.
[16] C. Colletto, S. Islam, F. Juliá-Hernández, I. Larrosa, *J. Am. Chem. Soc.* **2016**, *138*, 1677–1683.
[17] D.-T. D. Tang, K. D. Collins, J. B. Ernst, F. Glorius, *Angew. Chem. Int. Ed.* **2014**, *53*, 1809–1813.
[18] L.-Y. Liu, J. X. Qiao, W. R. Ewing, K.-S. Yeung, J.-Q. Yu, *Isr. J. Org. Chem.* **2020**, *60*, 416–418.
[19] M. Durai, L. Liu, P. Frère, T. Roisnel, V. Guerchais, H. Doucet, *Eur. J. Org. Chem.* **2023**, *26*, e202300303.
[20] D. Adamczak, H. Komber, A. Illy, A. Scaccabarozzi, M. Caironi, M. Sommer, *Macromolecules* **2019**, *52*, 7251–7259.
[21] E. Brier, C. Wetzel, M. Bauer, M. Wunderlin, P. Bäuerle, *Chem. Mater.* **2019**, *31*, 7007–7023.
[22] T. H. Nguyen, T. A. Nguyen, H. M. Tran, L.-T. T. Nguyen, A. T. Luu, J. Y. Lee, H. T. Nguyen, *Chem. Cent. J.* **2017**, *11*, 135.
[23] A. Dessi, D. A. Chalkias, S. Bilancia, A. Sinicropi, M. Calamante, A. Mordini, A. Karavioti, E. Stathatos, L. Zani, G. Reginato, *Sustain. Energy Fuels* **2021**, *5*, 1171–1183.
[24] S. C. Rasmussen, S. J. Evanson, *Prog. Polym. Sci.* **2013**, *38*, 1773–1804.
[25] J. Yuan, A. Gallagher, Z. Liu, Y. Sun, W. Ma, *J. Mater. Chem. A* **2015**, *3*, 2572–2579.
[26] J. Min, Y. N. Luponosov, D. A. Khanind, P. V. Dmitryakov, E. A. Svidchenko, S. M. Peregudova, L. Grodd, S. Grigorian, S. N. Chval, S. A. Ponomarenko, C. J. Brabec, *Org. Electron.* **2018**, *55*, 42–49.

© 2023 The Authors. Chemistry - A European Journal published by Wiley-VCH GmbH

15213765, 2023, 60, Downloaded from https://chemistry-europe.onlinelibrary.wiley.com/doi/10.1002/chem.202301867 by Universidad de la Rioja, Wiley Online Library on [29/11/2023]. See the Terms and Conditions (https://onlinelibrary.wiley.com/terms-and-conditions) on Wiley Online Library for rules of use; OA articles are governed by the applicable Creative Commons License

[27] X. Zhang, T. T. Steckler, R. R. Dasari, S. Ohira, W. J. Potscavage Jr, S. Prakash Tiwari, S. Coppée, S. Ellinger, S. Barlow, J.-L. Brédas, B. Kippelen, J. R. Reynolds, S. R. Marder, *J. Mater. Chem.* **2010**, *20*, 123–134.
[28] H.-I. Lu, C.-W. Lu, Y.-C. Lee, H.-W. Lin, L.-Y. Lin, F. Lin, J.-H. Chang, C.-I. Wu, K.-T. Wong, *Chem. Mater.* **2014**, *26*, 4361–4367.
[29] I. Ata, D. Popovic, M. Lindén, A. Mishra, P. Bäuerle, *Org. Chem. Front.* **2017**, *4*, 755–766.
[30] R. Sandoval-Torrientes, I. Zimmermann, J. Calbo, J. Aragó, J. Santos, E. Ortí, N. Martín, M. K. Nazeeruddin, *J. Mater. Chem. A* **2018**, *6*, 5944–5951.
[31] H.-L. Wong, C.-C. Ko, W. H. Lam, N. Zhu, V. W.-W. Yam, *Chem. Eur. J.* **2009**, *15*, 10005–10009.
[32] J. F. Mike, L. Shao, J.-W. Jeon, J. L. Lutkenhaus, *Macromolecules* **2014**, *47*, 79–88.
[33] P.-O. Schwartz, S. Förtsch, E. Mena-Osteritz, D. Weirather-Köstner, M. Wachtler, P. Bäuerle, *RSC Adv.* **2018**, *8*, 14193–14200.
[34] S. C. Rasmussen, E. J. Uzelac, E. W. C. Culver, *Adv. Heterocycl. Chem.* **2020**, *10*, 75–144.
[35] A. Vogt, F. Schwer, S. Förtsch, C. Lorenz, E. Mena-Osteritz, A. Aubele, T. Kraus, P. Bäuerle, *Chem. Eur. J.* **2021**, *27*, 12362–12370.
[36] C. Lorenz, A. Vogt, J. Millán, E. Mena-Osteritz, P. Bäuerle, *Org. Mater.* **2023**, *5*, 35–47.
[37] S. Förtsch, E. Mena-Osteritz, P. Bäuerle, *Polym. Chem.* **2021**, *12*, 3332–3345.
[38] J. P. Green, H. Dai, F. Aniés, M. Heeney, *Macromolecules* **2020**, *53*, 6649–6655.
[39] C. D. Wessendorf, G. L. Schulz, P. Kar, I. Ata, M. Weidelener, M. Urdanpilleta, J. Hanisch, E. Mena-Osteritz, M. Lindén, E. Ahlswede, A. Mishra, P. Bäuerle, *Adv. Energy Mater.* **2014**, *4*, 1400266.
[40] L. Ackermann, *Chem. Rev.* **2011**, *111*, 1315–1345.
[41] N. S. Gobalasingham, B. C. Thompson, *Prog. Polym. Sci.* **2018**, *83*, 135–201.
[42] a) L. G. Mercier, M. Leclerc, *Acc. Chem. Rev.* **2013**, *46*, 1597–1605; b) G. Albano, A. Punzi, M. A. M. Capozzi, G. Farinola, *Green Chem.* **2022**, *24*, 1809–1894.
[43] S. I. Gorelsky, D. Lapointe, K. Fagnou, *J. Am. Chem. Soc.* **2008**, *130*, 10848–10849.
[44] A. Berlin, G. Pagani, G. Zotti, G. Schiavon, *Macromol. Chem.* **1992**, *193*, 399–409.
[45] G. Sheldrick, *Acta Crystallogr. Sect. A Found. Crystallogr.* **2008**, *64*, 112–122.
[46] S. J. Evenson, T. M. Pappenfus, M. C. R. Delgado, K. R. Radke-Wohlers, J. T. L. Navarrete, S. C. Ramussen, *Phys. Chem. Chem. Phys.* **2012**, *14*, 6101–6111.
[47] S. C. Rasmussen, S. J. Evanson, *Prog. Polym. Sci.* **2013**, *38*, 1773–1804.
[48] a) S. Förtsch, P. Bäuerle, *Polym. Chem.* **2017**, *8*, 3586–3595; b) S. Förtsch, *PhD thesis*, University of Ulm (Germany), **2018**.
[49] C. Wetzel, E. Brier, A. Vogt, A. Mishra, E. Mena-Osteritz, P. Bäuerle, *Angew. Chem. Int. Ed.* **2015**, *54*, 12334–12338.
[50] R. Dorel, C. P. Grugel, A. M. Haydl, *Angew. Chem. Int. Ed.* **2019**, *58*, 17118–1729.
[51] R. Sato, T. Iida, T. Kanbara, J. Kuwabara, *Chem. Commun.* **2022**, *58*, 11511–11514.
[52] L. Wang, B. P. Carrow, *ACS Catal.* **2019**, *9*, 6821–6836.
[53] M. A. Campo, Q. Huang, T. Yao, Q. Tian, R. C. Larock, *J. Am. Chem. Soc.* **2003**, *125*, 11506–11507.
[54] We would explicitly like to thank the referees of the first version of this communication, who gave valuable comments to the proposed mechanism.
[55] *Handbook of Conducting Polymers*, 4th ed. (Eds.: J. R. Reynolds, B. C. Thompson, T. A. Skotheim), CRC Press, Boca Raton, **2019**.
[56] *CryaAlis^{Pro}*, Agilent Technologies XRD Products.
[57] L. J. Bourhis, O. V. Dolomanov, R. J. Gildea, J. A. K. Howard, H. Puschmann, *Acta Crystallogr. Sect. A Found. Adv.* **2015**, *71*, 59–75.
[58] O. V. Dolomanov, L. J. Bourhis, R. J. Gildea, J. A. K. Howard, H. Puschmann, *J. Appl. Crystallogr.* **2009**, *42*, 339–341.
[59] G. M. Sheldrick, *Acta Crystallogr. Sect. A Found. Crystallogr.* **2008**, *64*, 112.
[60] Gaussian 16, Revision C.01, M. J. Frisch, G. W. Trucks, H. B. Schlegel, G. E. Scuseria, M. A. Robb, J. R. Cheeseman, G. Scalmani, V. Barone, G. A. Petersson, H. Nakatsuji, X. Li, M. Caricato, A. V. Marenich, J. Bloino, B. G. Janesko, R. Gomperts, B. Mennucci, H. P. Hratchian, J. V. Ortiz, A. F. Izmaylov, J. L. Sonnenberg, D. Williams-Young, F. Ding, F. Lipparini, F. Egidi, J. Goings, B. Peng, A. Petrone, T. Henderson, D. Ranasinghe, V. G. Zakrzewski, J. Gao, N. Rega, G. Zheng, W. Liang, M. Hada, M. Ehara, K. Toyota, R. Fukuda, J. Hasegawa, M. Ishida, T. Nakajima, Y. Honda, O. Kitao, H. Nakai, T. Vreven, K. Throssell, J. A. Montgomery, Jr., J. E. Peralta, F. Ogliaro, M. J. Bearpark, J. J. Heyd, E. N. Brothers, K. N. Kudin, V. N. Staroverov, T. A. Keith, R. Kobayashi, J. Normand, K. Raghavachari, A. P. Rendell, J. C. Burant, S. S. Iyengar, J. Tomasi, M. Cossi, J. M. Millam, M. Klene, C. Adamo, R. Cammi, J. W. Ochterski, R. L. Martin, K. Morokuma, O. Farkas, J. B. Foresman, and D. J. Fox, Gaussian, Inc., Wallingford CT, **2016** .
[61] S. Förtsch, A. Vogt, P. Bäuerle, *J. Phys. Org. Chem.* **2017**, *30*, e3743.
[62] M. Shao, P. Dongare, L. N. Dawe, D. W. Thompson, Y. Zhao, *Org. Lett.* **2010**, *12*, 3050–3053.
[63] S. Förtsch, P. Bäuerle, *Polym. Chem.* **2017**, *8*, 3586–3595.
[64] V. Nikolova, D. Cheshmedzhieva, S. Ilieva, B. Galabov, *J. Org. Chem.* **2019**, *84*, 1908–1915.
[65] S. Liu, *J. Chem. Phys.* **2014**, *141*, 194109.

Manuscript received: June 12, 2023
Version of record online: September 4, 2023

© 2023 The Authors. Chemistry - A European Journal published by Wiley-VCH GmbH

15213765, 2023, 60, Downloaded from https://chemistry-europe.onlinelibrary.wiley.com/doi/10.1002/chem.202301867 by Universidad de la Rioja, Wiley Online Library on [29/11/2023]. See the Terms and Conditions (https://onlinelibrary.wiley.com/terms-and-conditions) on Wiley Online Library for rules of use; OA articles are governed by the applicable Creative Commons License